GPS Solut (2012) 16:375–387
DOI 10.1007/s10291-011-0239-3

ORIGINAL ARTICLE

Approach service type D evaluation of the DLR GBAS testbed

Thomas Dautermann · Michael Felux · Anja Grosch

Received: 26 May 2011 / Accepted: 27 July 2011 / Published online: 8 September 2011

Abstract Ground-based augmentation systems (GBAS) for satellite navigation are intended to replace the instrument landing system for precision approach of aircraft into an airport in the near future. Here, we show an evaluation of data collected during flight trials with the GBAS testbed of the German aerospace center with respect to requirements for the GBAS approach service type D. This service will permit approach and landing down to the zero visibility conditions of category IIIc approaches. We show output of all airborne monitors and the results of an integrity analysis. During all flight trials, the system performed within the required criteria for integrity, continuity, and availability.

Keywords GBAS · Flight trials · Integrity · GAST-D

Introduction

The instrument landing system (ILS) has been safely guiding aircraft on the final approach for about 70 years and is by far the most important and most often used guidance system for landings. It consists of two VHF transmitters of which one provides lateral and the other vertical guidance. Both transmitters are necessary for each runway end to which precision approach is provided. This makes the system expensive because multiple installations are necessary at one airport. Furthermore, the design only allows the definition of straight-in approach trajectories to a fixed point, which makes operations inflexible. As an ILS-successor, the microwave landing system (MLS) was developed in the 1980s. It allows more flexibility, mainly by allowing the definition of multiple approach tracks to one runway threshold. However, the development was ceased when global navigation satellite systems (GNSS) with augmentation were expected to be capable of providing safe and reliable guidance with greatly improved flexibility in the definition of approach tracks. Moreover, these systems were expected to be more cost effective since usually only one reference system at each airport is necessary.

A consortium of Stanford University, Boeing, United Airlines and the US Federal Aviation Administration began development of a satellite-based guidance system that culminated in the successful completion of flight trials in 1994 when a Boeing 737 performed a series of automatic landings based only on GNSS navigation (Cohen et al. 1995). Here, a differential GPS (DGPS) system in conjunction with pseudolites (called integrity beacons) provided the necessary accuracy and integrity for guidance all the way to touchdown. However, development of the pseudolite concept was discontinued mainly due to the "near–far problem" of strong signal power variations during an approach (Ndili 1994). Since then the concept of a ground-based augmentation system (GBAS), also called local area augmentation system (LAAS) in the US, changed and no longer contains pseudolites, but consists of typically three to four reference antennas at the airport (Satkunanathan and Murphy 1998). In contrast to the Integrity Beacon Landing System, the ground station now has to provide differential corrections and ensure accuracy, integrity, continuity, and availability at the same time (Enge 1999). This task is not easily accomplished because the system has to protect the user against a wide variety of

T. Dautermann (✉) · M. Felux · A. Grosch
Deutsches Zentrum für Luft- und Raumfahrt e.V.,
Institute of Communications and Navigation,
Oberpfaffenhofen, 82234 Wessling, Germany
e-mail: thomas.dautermann@dlr.de

possible failures. Many different failures and possible threats to the system that had previously been observed were studied, and appropriate detection and mitigation strategies were discussed. They include satellite signal faults (Mitelman et al. 1999; Pullen et al. 2002), satellite orbit issues (Pervan and Chan 2003; Gratton et al. 2004), ground subsystem failures, and receiver multipath (Lee et al. 2001; Normark et al. 2002) as well as ionospheric anomalies that can cause significant differential ranging errors (Lee et al. 2007). From all these threats to a GBAS, an integrity concept using protection levels was derived. The protection levels bound the positioning error with a given probability (0.5×10^{-7} for GBAS approach service type D as defined ICAO NSP 2010). Boeing obtained certification for the airborne equipment in May 2005 with a 737NG (Murphy et al. 2006), and in 2009, Honeywell received System Design Approval by the FAA (Honeywell 2009; FAA 2005) for a GBAS ground station supporting CAT-I (GBAS approach service type C) operations. In October 2007, a special CAT-I system was certified for precision approaches in Norway. It has the same components and provides the same kind of service as a standard GBAS but is restricted to one manufacturer for the ground stations and one for the corresponding avionics in equipped aircraft (FAA 2003). However, for weather conditions below the CAT-I minima (decision height 200 ft and runway visual range 550 m), this architecture cannot provide sufficient protection against ionospheric anomalies (Dautermann and Mayer 2010; Luo et al. 2004). Standards for GAST-C are governed by the relevant documents of EUROCAE ED114 (2003) and RTCA DO245A (2004), RTCA DO253C (2008), and RTCA DO246D (2009).

Presently, the draft requirements for the GBAS approach service type D (GAST-D), which is intended to support operations below the CAT-I minima, are under discussion at ICAO. These include additional low-level monitoring requirements such as a ground-based absolute ionospheric gradient monitor as, for example, proposed by Khanafseh et al. (2010) and airborne dual solution ionospheric gradient monitoring architecture (abbreviated as DSIGMA, Murphy and Harris 2006), as well as an extended protection level concept (Shively and Hsiao 2010).

The German Aerospace Center DLR has set up an experimental GBAS station at the research airport in Braunschweig, Germany, and conducted flight trials in 2009 to evaluate the system performance and proposed algorithms in a real-world environment. Here, we present post-processed results of these flight trials and an evaluation of the GBAS testbed with respect to the GAST-D parameters and requirements. In the evaluation, we use the existing standardization documents RTCA DO253c and the ICAO SARPs and point out discrepancies and errors among them.

Fig. 1 The advanced technology aircraft testing system ATTAS in flight. The location of the GPS antenna is indicated by the *red arrow*

For the flight trials, we used DLR's ATTAS (Advanced Technologies Transport Aircraft System) VFW 614 research aircraft. The aircraft is a twin jet that has been operated by the DLR since 1985. The ATTAS has a typical approach speed of 157 km/h and minimum landing distance of 620 m. The GNSS antenna is located in the center of the midsection of the fuselage next to one of the VHF antennas (Fig. 1).

During 2009, thirty approaches were conducted while the GPS receivers were operational. The exact dates of the trials are given in Table 4. Figure 7 shows the top view of typical approaches within the GBAS service volume.

Ground facility and ground processing

The GBAS ground facility at the research airport Braunschweig/Wolfsburg (ICAO Identifier EDVE) consists of three Topcon Net-G3 dual frequency receivers with Leica AR25 choke ring antennas underneath a radome. Figure 2 shows an aerial photograph, and Table 1 gives the coordinates of the antennas. The receivers are located in three shelters on the airport property with baselines of 740.75 m (BR02, BR03), 766.45 m (BR01, BR03), and 775.49 m (BR01, BR02), respectively. All ground receivers are connected to a Temex LPFRS reference oscillator to improve short-term clock stability. During the flight trials, we configured the receivers to record only GPS data at a rate of 20 Hz, which was then down-sampled to 2 Hz to process the GBAS ground corrections. Guidance for civil aircraft can only be provided by navigation signals that are located within the protected aeronautical frequency bands. As such, it is only permitted to use the L1 signal for navigation purposes. Thus, for the navigation algorithms presented here, we use only the civilian signal on L1.

The ground subsystem processes the measured pseudoranges and monitors the GNSS signal in space. First, in

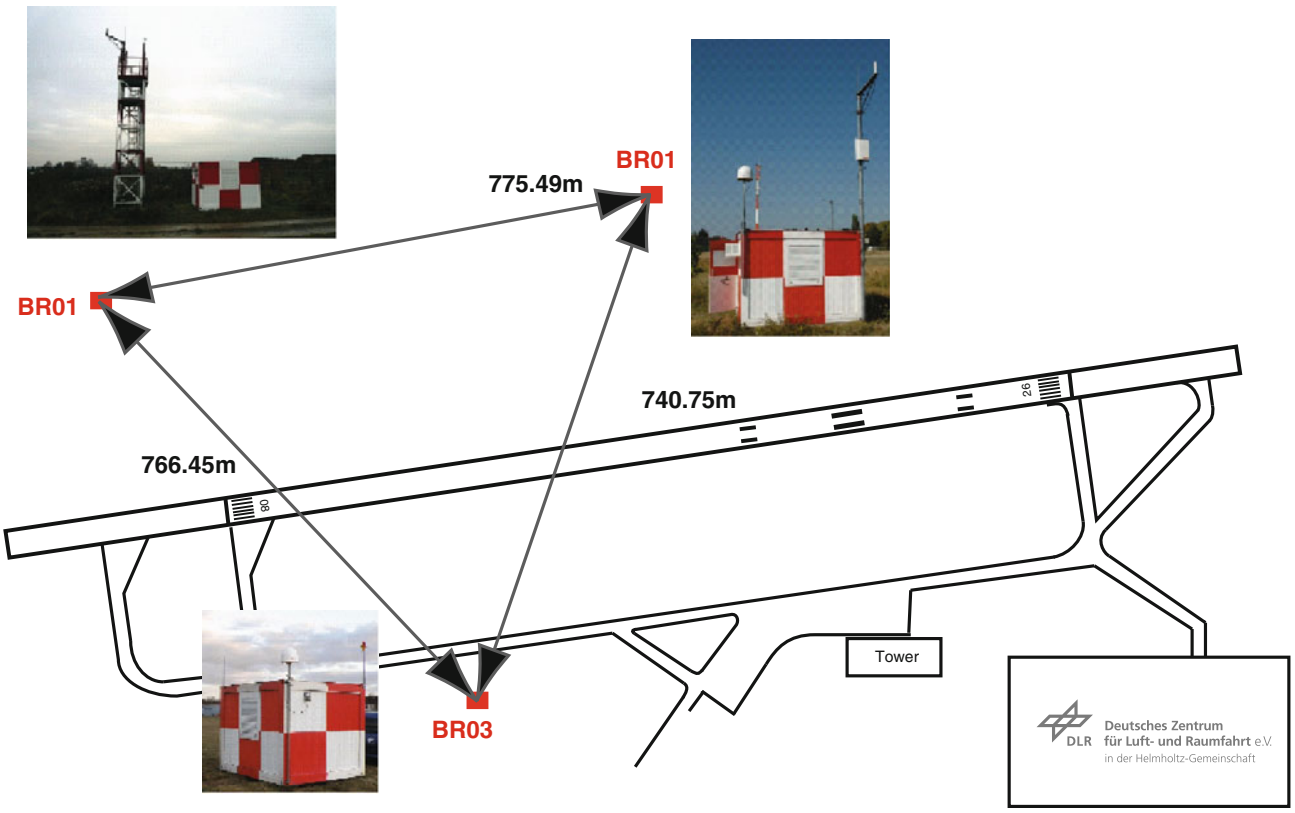

Fig. 2 GBAS siting at Braunschweig airport

Table 1 GBAS antenna locations

Receiver	Latitude [°]	Longitude [°]	Altitude [m]
BR01	52° 19′ 17.1948″N	10° 32′ 36.0096″E	131.421
BR02	52° 19′ 20.3664″N	10° 33′ 16.6242″E	133.140
BR03	52° 18′ 58.1538″N	10° 33′ 1.93620″E	131.170

order to reduce the measurement noise, the raw pseudoranges are smoothed using a Hatch filter.

$$\hat{\rho}_n = \alpha\rho_n + (1-\alpha)\left(\hat{\rho}_{n-1} + \frac{\lambda}{2\pi}(\phi_n - \phi_{n-1})\right) \quad (1)$$

where ρ_n is the raw pseudorange, $\hat{\rho}_n$ is the smoothed pseudorange, $\lambda = 0.1905$m is the L1 wavelength, ϕ_n is the carrier phase in radians, and $\alpha = 0.5\ \mathrm{s}/\tau$ is the filter weighting constant, which is equal to the sample interval divided by the filter time constant τ. For a GAST-D ground station, two filters with time constants $\tau = 100$ s and $\tau = 30$ s are operated in parallel for each receiver. At each individual receiver j, pseudorange correction (PRC) for each satellite i and smoothing time constant are determined using

$$\mathrm{PRC}(i,j) = r_{i,j} - \hat{\rho}_{i,j} - c\Delta t_{sv,i} \quad (2)$$

where $r_{i,j}$ is the true range from receiver j to satellite i and $c\Delta t_{sv,i}$ is the satellite clock correction from the navigation message (IS-GPS-200D 2004). Since each pseudorange measurement is affected by the receiver clock bias, the PRCs are adjusted accordingly for each receiver as.

$$\mathrm{PRC}_{\mathrm{SCA}}(i,j) = \mathrm{PRC}(i,j) - \sum_{i=1}^{N} k_i \mathrm{PRC}(i,j) \quad (3)$$

with the requirement that $\sum k_i = 1$. This smooth clock adjust (SCA) is necessary to compare the pseudorange corrections between receivers as each receiver has a different receiver clock offset. We have chosen a linear elevation weighting where the weights are given as $k_i = \theta_i / \sum_i^N \theta_i$ for N satellites tracked at elevation angle θ_i. Lastly, the PRCs that are transmitted through the datalink are averaged between all receivers M that track a given satellite:

$$\mathrm{PRC}_{\mathrm{TX}}(i) = \frac{1}{M(i)} \sum_j \mathrm{PRC}(i,j)_{\mathrm{SCA}} \quad (4)$$

Additionally, the data are monitored by a code carrier divergence monitor (Simili and Pervan 2006; RTCA

DO253C 2008), which uses two first-order linear time invariant filters with a weighting constant of $\alpha = 0.5\ \text{s}/100\ \text{s} = 1/200$. The filter differentiates the code minus carrier observable CMC and applies a low pass to reduce the receiver noise:

$$\Delta\text{CMC}_n = \frac{1}{0.5\text{s}}\left(\left(\rho_n - \frac{\lambda}{2\pi}\phi_n\right) - \left(\rho_{n-1} - \frac{\lambda}{2\pi}\phi_{n-1}\right)\right) \tag{5}$$

$$Z_n = (1-\alpha)Z_{n-1} + \alpha\Delta\text{CMC}_n \tag{6}$$

$$D_n = (1-\alpha)D_{n-1} + \alpha Z_n. \tag{7}$$

The result is compared to a threshold of 0.0125 m/s, and the respective satellite is flagged and taken out of the pseudorange correction computation if the threshold is exceeded.

In order to protect against a faulty measurement, the PRC_{SCA} from each receiver are checked against each other by computing B-values. For each receiver–satellite pair, the $B(i,j)$ is computed using

$$B(i,j) = \text{PRC}_{\text{TX}}(i) - \frac{1}{M(i)-1}\sum_{k\neq j}\text{PRC}_{\text{SCA}}(i,k), \tag{8}$$

i.e. it is the difference between the broadcast PRC and the PRC obtained by excluding the receiver j. If the B-value exceeds the preset limit of

$$B(i,j) > \frac{K_B\sigma_{\text{pr,gnd};i}}{\sqrt{M-1}} \tag{9}$$

a reference receiver fault is declared and no B-value for that satellite–receiver pair will be broadcast. In Eq. (9), K_B is a station configurable parameter between 5 and 6 that can be selected by the manufacturer in order to meet the continuity requirements. We chose $K = 5$ to be most conservative for the evaluation presented in this manuscript.

In the nominal case, i.e., without reference receiver fault, the computed B-values can be used to assess the accuracy of the ground subsystem through their standard deviation. The standard deviation of the B-values σ_B is related to the standard deviation of the carrier-smoothed pseudoranges $\sigma_{\text{pr,gnd}}$ by

$$\sigma^2_{\text{pr,gnd}} = \sigma^2_B\frac{(M-1)(N+1)}{N} \tag{10}$$

where N is the number of satellites used and M the number of reference receivers ($M = 3$ in our case).

Each ground subsystem can be classified into three categories called ground accuracy designator (GAD) A, B, and C using the determined $\sigma_{\text{pr,gnd}}$ as given in the standardization document for the ground subsystem RTCA DO245A (2004). A detailed review and description of these ground and airborne accuracy models can be found in McGraw et al. (2000).

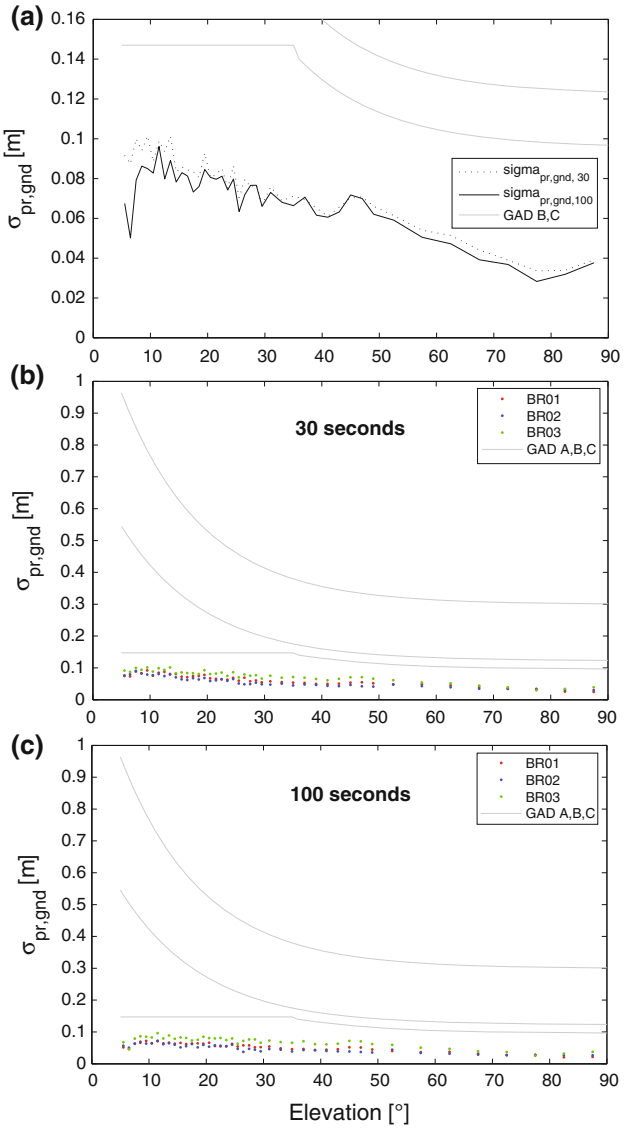

Fig. 3 This figure shows the assessment of the ground accuracy designator GAS. **a** Comparison of the $\sigma_{\text{pr,gnd}}$ for message type 11 with $\sigma_{\text{pr,gnd}}$ derived for message type 2. The gray curves show the requirements for GAD B (middle) and GAD C (bottom). (b) GAD assessment for 24 h data from day 318 of 2009 and a 30 s code-carrier smoothing. The bins have a spacing of 1° up to 30° elevation, 2° between 30° and 50° elevation, and 5° from 50° to 90°. (c) GAD assessment for 24 h data from day 318 of 2009 and a 100 s code-carrier smoothing. The bins have a spacing of 1° up to 30° elevation, 2° between 30° and 50° elevation, and 5° from 50° to 90°

For the station in Braunschweig, we performed this GAD determination using B-values computed with a time constant of $\tau = 30\text{s}$ as well as with B-values computed with a time constant of $\tau = 100\text{s}$, both recorded on day 318 of 2009 (one sidereal day in accordance with the standards). Thus, unlike the FAA LAAS test prototype, we do not need to use an inflated version of the $\sigma_{\text{pr,gnd}}$ determined for the 100 s smoothing filter (Murphy et al. 2010). In order to have independent data, we used only one sample

Table 2 Message type 2 parameters

MT2 parameter	Value
GCID	6
SigmaVertIonoGradient	4 mm/km
SigmaVertIonoGradient D	4 mm/km
Refractivity index	379
Scale height	7949.42
Refractivity uncertainty	20
Latitude	52° 19′ 17.1840″N
Longitude	10° 32′ 36.0996″E
Ellipsoid height	130
RSDS	1
Dmax	38
KmdeCAT1GPS	5.810

Table 3 Message type 4 parameters

MT4 parameter	Value
NUMFAS	1
FASVALAS	10 m
FASLALAS	40 m
Operation type	0
SBAS provider	0
Airport ID	EDVE
Runway number	28
Runway letter	0
APD	1
Route indicator	“A”
RPDS	6
Reference path ID	“TES1”
LTPFTP latitude	52° 19′ 10.7112″N
LTPFTP longitude	10° 33′ 50.4210″E
LTPFTP height	130
dFPAP latitude	−0° 0′ 3.5280″N
dFPAP longitude	−0° 1′ 3.0612”E
TCH	15
Approach TCH units selector	1
GPA	3
Course width threshold	80
Length offset	0

every 2τs. The data were evaluated in bins of varying width depending on the elevation angle, i.e., width 1° from 5 to 30°, width of 2° from 30 to 50° elevation, and a bin width of 5° from 50 to 90° of elevation. The results are shown in Fig. 3b for the 30 s smoothing and in Fig. 3c for the 100 s smoothing. For the Braunschweig testbed, we can see that the $\sigma_{\mathrm{pr,gnd}}$ for both smoothing times is largest for site BR03, which is located closely to several hangar buildings. The value of $\sigma_{\mathrm{pr,gnd}}$ that is broadcast for each elevation is the maximum obtained over all stations. Figure 3a shows the final broadcast values of $\sigma_{\mathrm{pr,gnd,30s}}$ and $\sigma_{\mathrm{pr,gnd,100s}}$. In both cases, the values are below the GAD C curve and the values obtained for $\tau = 100$s are smaller than the ones for the 30 s smoothing constant. In accordance with Murphy et al. (2010), the gain in accuracy by using a filter constant of 100 s compared to 30 s is well below the theoretically derived value of $\sqrt{100/30} = 1.826$.

For a GAST-D ground system, the $\sigma_{\mathrm{pr,gnd}}$ for the 30 s time constant is contained within the message type 11, which is required in addition to the GAST-C message type 2. Message type 11 also contains pseudorange and range rate corrections that were computed with the 30 s hatch filter. The message type 2 and message type 4 constants that we used for the post-processing are given in Tables 2 and 3. A detailed overview of the data transmitted within the individual message types can be found in RTCA DO246D (2009).

Board processing and implementation

The receiver on board the aircraft was also a Topcon Net-G3 running only on an internal quartz oscillator. Airborne data were also recorded at 20 Hz and then down-sampled during post-processing to 2 Hz. A schematic overview of the onboard processing architecture is shown in Fig. 4.

Positioning and protection levels

As for the GBAS ground system, the raw pseudoranges measured on board the aircraft are smoothed using the measured carrier phase. Two code-carrier smoothing filters are also operated in parallel on board the aircraft with time constants of $\tau = 100$s and $\tau = 30$s. The smoothed pseudoranges are subsequently corrected using

$$\rho_{\mathrm{corrected}} = \hat{\rho} + \mathrm{PRC} + \mathrm{RRC}(t - t_{\mathrm{apl}}) + \mathrm{TC} + c\Delta t_{\mathrm{sv}} \quad (11)$$

where $\rho_{\mathrm{corrected}}$ is the corrected pseudorange, $\hat{\rho}$ the carrier-smoothed pseudorange, PRC the pseudorange correction, and RRC the range rate correction from message type 1. The time of applicability of the PRC is denoted by t_{apl}, and TC is the tropospheric correction and Δt_{sv} the satellite clock correction from the navigation message. The tropospheric correction is computed according to the RTCA DO253C as

$$\mathrm{TC} = N_{\mathrm{R}} h_0 \frac{10^{-6}}{\sqrt{0.002 + \sin^2\theta}} \left(1 - \mathrm{e}^{-\frac{\Delta h}{h_0}}\right) \quad (12)$$

with Δh the height difference between the GBAS reference point and the aircraft, and θ the elevation angle of the

Table 4 Overview of all approaches flown during the 2009 flight trails

Date	No. approaches
11/16/2009	4
11/26/2009	1
11/27/2009	4
12/07/2009	6
12/11/2009	6
12/14/2009	2
12/16/2009	7

satellite. The parameters N_R and h_0 denote the refractivity index and tropospheric scale height from the type two message (Table 2). The position solution is computed using the linearization

$$\Delta\rho_{\text{corrected}} = G\Delta x \tag{13}$$

around the a priori position estimate. The solution is a weighted least squares result

$$\Delta\hat{x} = (G^T WG)^{-1} G^T W \Delta\rho_{\text{corrected}} \tag{14}$$

with the weighting matrix W and the pseudoinverse $S = (G^T WG)^{-1} G^T W$. The matrix $\mathbf{G_i} = [-\mathbf{e_i^T} \quad 1]$ is the well-known geometry matrix and contains the unit vector to each usable satellite i in view. The weighting matrix is a diagonal matrix and contains the variances of the measurement error for each satellite,

$$W_{ii} = \sigma_i^{-2} \tag{15}$$

where σ_i is the standard deviation of error distribution associated with an error in the measurement from satellite i, with

$$\sigma_i^2 = \sigma_{\text{pr,gnd},x;i}^2 + \sigma_{\text{tropo},i}^2 + \sigma_{\text{pr,air};i}^2 + \sigma_{\text{iono},i}^2 \tag{16}$$

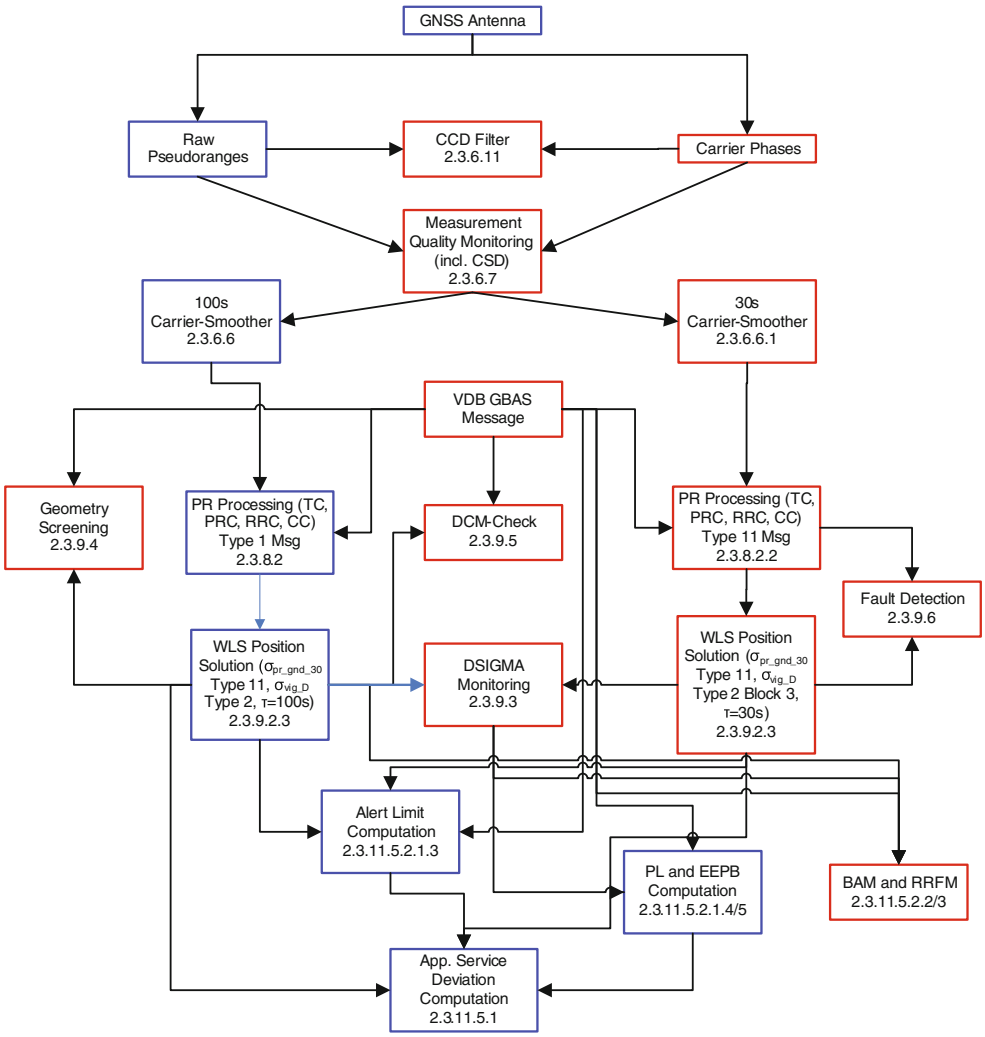

Fig. 4 Architecture of the aircraft subsystem. The chapter number of the relevant MOPS section of RTCA DO253C (2008) is indicated. The GAST-D extension is indicated by *red box*. Legacy GAST-C is shown in *blue*

where $\sigma^2_{\text{tropo},i}$ describes the residual tropospheric uncertainty and $\sigma^2_{\text{pr,air};i}$ is the post-correction fault-free airborne multipath and receiver noise error. Both $\sigma^2_{\text{iono},i}$ and $\sigma^2_{\text{pr,gnd},x}$ depend on the approach service type that is currently in use. For GAST-C, the $\sigma^2_{\text{pr,gnd},x,i}$ is taken from message type 1 and the $\sigma^2_{\text{iono},i}$ is based on the transmitted $\sigma_{\text{vert\_iono\_gradient},C}$ from message type 2 (both obtained from 100s smoothed data). For GAST-D, the $\sigma^2_{\text{pr,gnd},x,i}$ is taken from message type 11 and the $\sigma^2_{\text{iono},i}$ is based on the transmitted $\sigma_{\text{vert\_iono\_gradient},D}$ from the message type 2 additional data block (both obtained from 30s smoothed data). The σ_{iono} is computed based on the distribution of the nominal ionospheric gradient $\sigma_{\text{vert\_iono\_gradient}}$ and elevation mapping function F_{PP}, the distance x_{air} between the aircraft and the GBAS reference point, the horizontal speed v_{air}, and the smoothing time constant τ, as

$$\sigma_{\text{iono}} = F_{\text{PP}}\sigma_{\text{vert\_iono\_gradient}}(x_{\text{air}} + 2\tau v_{\text{air}}). \tag{17}$$

Thus, in the case when $\sigma_{\text{vert\_iono\_gradient},C} = \sigma_{\text{vert\_iono\_gradient},D}$, the ionospheric error standard deviation for GAST-D is smaller than for GAST-D. In our case, we used for both a value of 4 mm/km—the inflated value determined for the CONUS region. The protection levels will be more conservative, since this value has been inflated to provide additional safety margin (Pullen 2000; Luo et al. 2002; Datta-Barua et al. 2002). Thus, when the aircraft is far from the GBAS ground facility, we have $\sigma_{i,\text{GAST}-D} < \sigma_{i,\text{GAST}-C}$. As it approaches the airport, the influence of σ_{iono} diminishes and $\sigma_{i,\text{GAST}-D}$ may become larger than $\sigma_{i,\text{GAST}-C}$ due to the higher value of $\sigma^2_{\text{pr,gnd},x}$.

In order to protect the user during the critical approach phase, the system integrity is measured by comparing vertical and lateral protection levels to the respective alert limit. These protection levels are based on the required integrity risk from the standardization documents. The alert limits vary with the distance of the approaching aircraft to the landing threshold point (LTP). The lateral alert limit (LAL) shrinks from 69.15 m to the final approach segment lateral alert limit (FASLAL) of 40 m. The vertical alert limit (VAL) diminishes from 43.35 m to the final approach segment vertical alert limit (FASVAL) of 10 m. Details on the computation can be found in RTCA DO253C Tables 2-14 and 2-15.

The vertical and lateral protection levels for approach service are computed as the maximum out of two hypothesis H_0 and H_1, where H_0 is the nominal case and H_1 assumes a single reference receiver fault.

$$\text{LPL}_{\text{Apr}} = \max[\text{LPL}_{\text{Apr},H0}, \text{LPL}_{\text{Apr},H1}] \tag{18}$$

$$\text{VPL}_{\text{Apr}} = \max[\text{VPL}_{\text{Apr},H0}, \text{VPL}_{\text{Apr},H1}] \tag{19}$$

The nominal protection levels are computed as

$$\text{VPL}_{\text{Apr\_}H0} = K_{\text{ffmd}}\sqrt{\sum_{i=1}^{N} S^2_{\text{Apr,vert},i}\sigma_i^2} + D_{\text{V}} \tag{20}$$

$$\text{LPL}_{\text{Apr\_}H0} = K_{\text{ffmd}}\sqrt{\sum_{i=1}^{N} S^2_{\text{Apr,lat},i}\sigma_i^2} + D_{\text{L}} \tag{21}$$

with the fault-free missed detection multiplier K_{ffmd}, which equals 5.81 for three ground receivers, N the number of satellites used, S the elements of the approach type-dependent pseudoinverse S from (14), and D_{L} and D_{V} are the magnitude of the vertical and lateral projection of the difference between the 30 and 100 s smoothed position. The reference receiver fault protection levels are determined by the maximum over each receiver

$$\text{VPL}_{\text{Apr},H1} = \max[\text{VPL}_{\text{Apr},H1}(j)] + D_{\text{V}} \tag{22}$$

$$\text{LPL}_{\text{Apr},H1} = \max[\text{LPL}_{\text{Apr},H1}(j)] + D_{\text{L}} \tag{23}$$

with

$$\text{VPL}_{\text{Apr},H1}(j) = \left|\sum_{i=1}^{N} S_{\text{Apr,vert},i}B(i,j)\right| + K_{\text{md}}\sqrt{\sum_{i=1}^{N} S^2_{\text{Apr,vert},i}\sigma^2_{i,H1}} \tag{24}$$

$$\text{LPL}_{\text{Apr},H1}(j) = \left|\sum_{i=1}^{N} S_{\text{Apr,lat},i}B(i,j)\right| + K_{\text{md}}\sqrt{\sum_{i=1}^{N} S^2_{\text{Apr,lat},i}\sigma^2_{i,H1}} \tag{25}$$

with the missed detection multiplier K_{md} (2.898 for three receivers). In order to calculate the standard deviation $\sigma_{i,H1}$ of the H1 case, the $\sigma_{\text{pr,gnd},x;i}$ of (16) is inflated by a factor of 1.5 (for three operational reference receivers).

The ICAO SARPs are inconsistent with the calculation of the σ_i for GAST-D Service: When GAST-D is active, two different smoothing times of 30 and 100 s are used and, based on them, two position solutions with the same weighting matrix are formed. The weighting matrix for both position solutions is a diagonal matrix with the inverse of an estimated variance for each satellite as entries. These variances are defined by (16). Approach guidance is accomplished using 30 s smoothed pseudoranges with corrections and integrity parameters from the type 11 message provided by the GBAS ground subsystem (ICAO NSP 2010, Section 7.19.3). The $\sigma_{\text{iono},i}$ is calculated according to (17) with $\tau = 30\text{s}$, and $\sigma_{\text{pr,gnd},x;i}$ is defined as $\sigma_{\text{pr,gnd},30;i}$ from message type 11 (ICAO NSP 2010, Sect. 3.6.5.4). However, when the variances are used for the

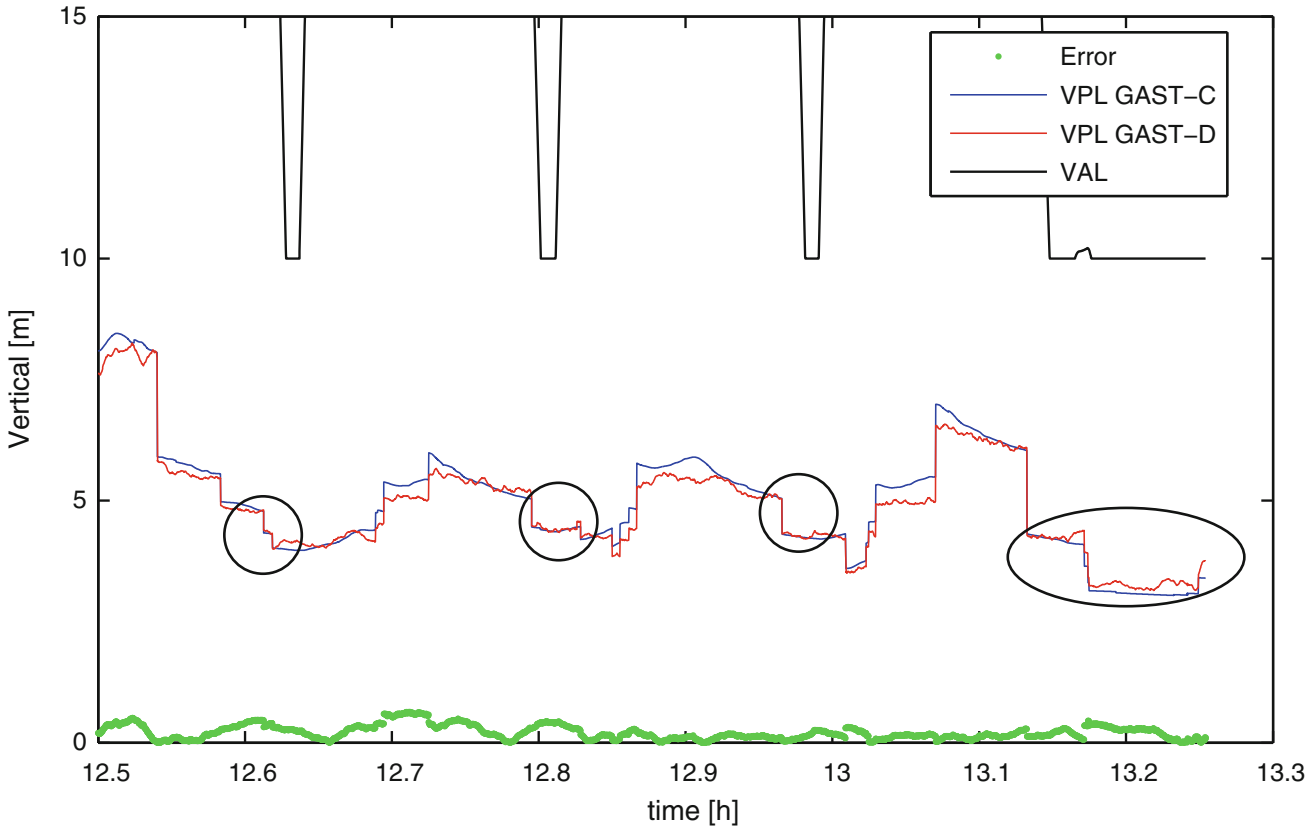

Fig. 5 Temporal evolution of the vertical in FE16. The *black circles* indicate the protection levels during the four approaches. The GAST-D protection level is larger than the GAST-C protection level as the aircraft approaches the ground facility

GAST-D protection level calculations, different parameters are applied. The individual variances are still defined as given by (16), but now, $\sigma_{\text{iono},i}$ is calculated with $\tau = 100$s and $\sigma_{\text{pr,gnd},x;i}$ is defined as $\sigma_{\text{pr,gnd},D;i}$ from message type 11. The $\sigma_{\text{pr,gnd},D}$ is defined as *"..the standard deviation of a normal distribution associated with the signal-in-space contribution of the pseudorange error in the 100 s smoothed correction in the Type 1 message at the GBAS reference point."* by the baseline standards and recommended practises ICAO NSP (2010), Section 3.6.4.11.4 with the special condition that *"The parameter* $\sigma_{\text{pr\_gnd\_}D}$ *differs from* $\sigma_{\text{pr\_gnd}}$ *for the corresponding measurement in the Type 1 message in that* $\sigma_{\text{pr\_gnd\_}D}$ *should include no inflation to address overbounding of decorrelated ionospheric errors."*

However, the protection levels are an instantaneous characterization of the position error distribution based on nominal error distributions of the individual error components. This fact is no longer given in the current version of the SARPs. If weights, pseudoranges, and corrections based on a 30 s smoothing time are used in the positioning service, they should also be used for the protection levels. For this reason, we decided to use the more logical approach and use the 30 s parameters in the GAST-D protection level calculations.

Onboard monitors

In addition to the ground monitoring, GAST-D requires additional provisions for airborne monitoring of the satellite signals and observables. For example, the code carrier divergence monitoring algorithm is duplicated at the airborne side and identical to the one given by (7). In this section, we describe the additional monitors in more detail.

Dual solution ionospheric gradient monitoring architecture (DSIGMA)

For airborne ionosphere monitoring during a GAST-D approach, two position solutions are generated using the weighting matrix W based on the 30 s sigmas. One employs corrections from message type 1, which are based on the 100 s smoothed pseudoranges; the other uses pseudorange corrections from the 30 s smoothed data, which are transmitted in message type 11. The dual solution ionospheric gradient monitoring (Murphy and Harris

2006) compares the difference in vertical and horizontal position between the two solutions and degrades the available approach service type to GAST-C, should this difference exceed 2 m.

Differential correction magnitude check (DCMC)

The airborne equipment compares the horizontal projection of the differential correction magnitude (DCM) in the position domain with a threshold of 200 m (RTCA DO253C, section 2.3.9.5). The horizontal projection DCM_H is given by

$$\mathrm{DCM}_H = \sqrt{x_1^2 + x_2^2} \tag{26}$$

where $\vec{x}$ is given by

$$\vec{x} = S\delta\mathrm{PR} \tag{27}$$

with the pseudoinverse S from (14) and the vector of corrections defined as

$$\delta\mathrm{PR}_i = \mathrm{PRC}_i + \mathrm{RRC}_i(t - t_{\mathrm{apl}}) + \mathrm{TC}_i \tag{28}$$

Note that RTCA DO253C (2008) also includes the satellite clock correction term $c\Delta t_{\mathrm{sv},i}$ as part of the correction that is used in the differential correction magnitude check. This quantity, however, is usually around 5 to 10 km of magnitude and would always lead to a flag in the DCM monitor. Since this cannot be the purpose of this monitor, we operate this algorithm without the satellite clock correction term.

Geometry screening

The aircraft subsystem continuously screens satellite geometry of the available satellites to ensure that the projection of individual pseudorange errors into the position domain does not become too large. This is accomplished by limiting the magnitude of individual elements of the pseudoinverse S to a maximum value $S_{\max}$. The derivation of $S_{\max}$ depends on the flight technical error of the aircraft, which is being certified for GAST-D approaches. A detailed discussion can be found in Burns et al. (2009). Here, we limit the magnitude of the individual elements of S to a maximum value of 4.

Bias approach monitor (BAM)

Upon transitioning into the precision approach region (PAR) and when the set of satellites being used changes while inside the PAR, the airborne subsystem tests for

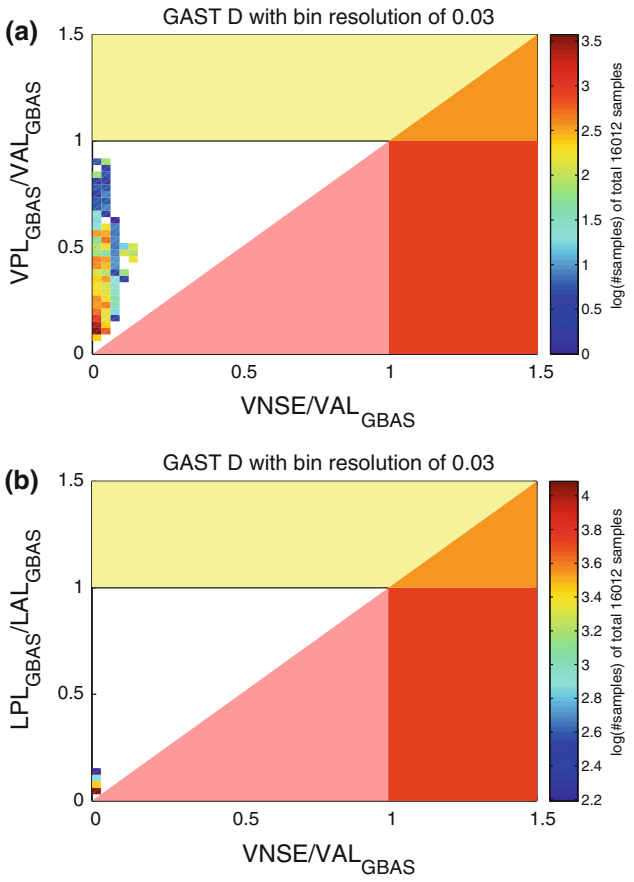

Fig. 6 Integrity assessment using the data collected from inside the GBAS precision approach region as shown in Fig. 5a Vertical integrity plot for all approaches. **b** Lateral integrity plot for all approaches

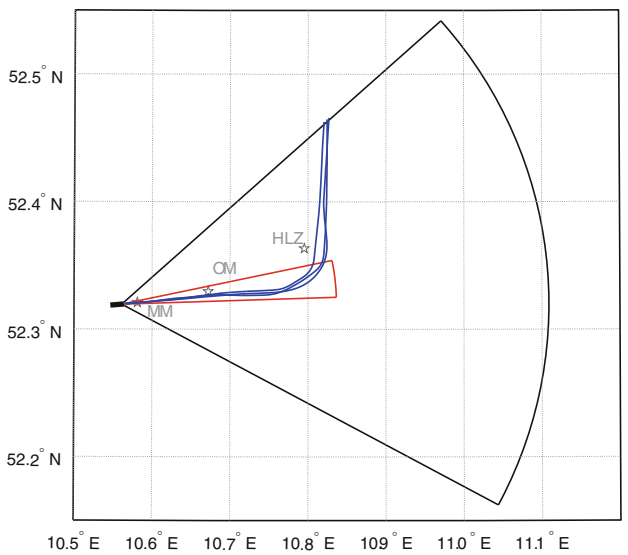

Fig. 7 Map of the approach paths for the flight trials on Dec 7, 2009. MM and OM denote the position of the middle and outer marker of the ILS RW26 approach at Braunschweig Airport EDVE. HLZ is the position of the Hehlingen VORTAC. The GBAS service area is indicated by the *black wedge*, and the precision approach region is inside the *red area*

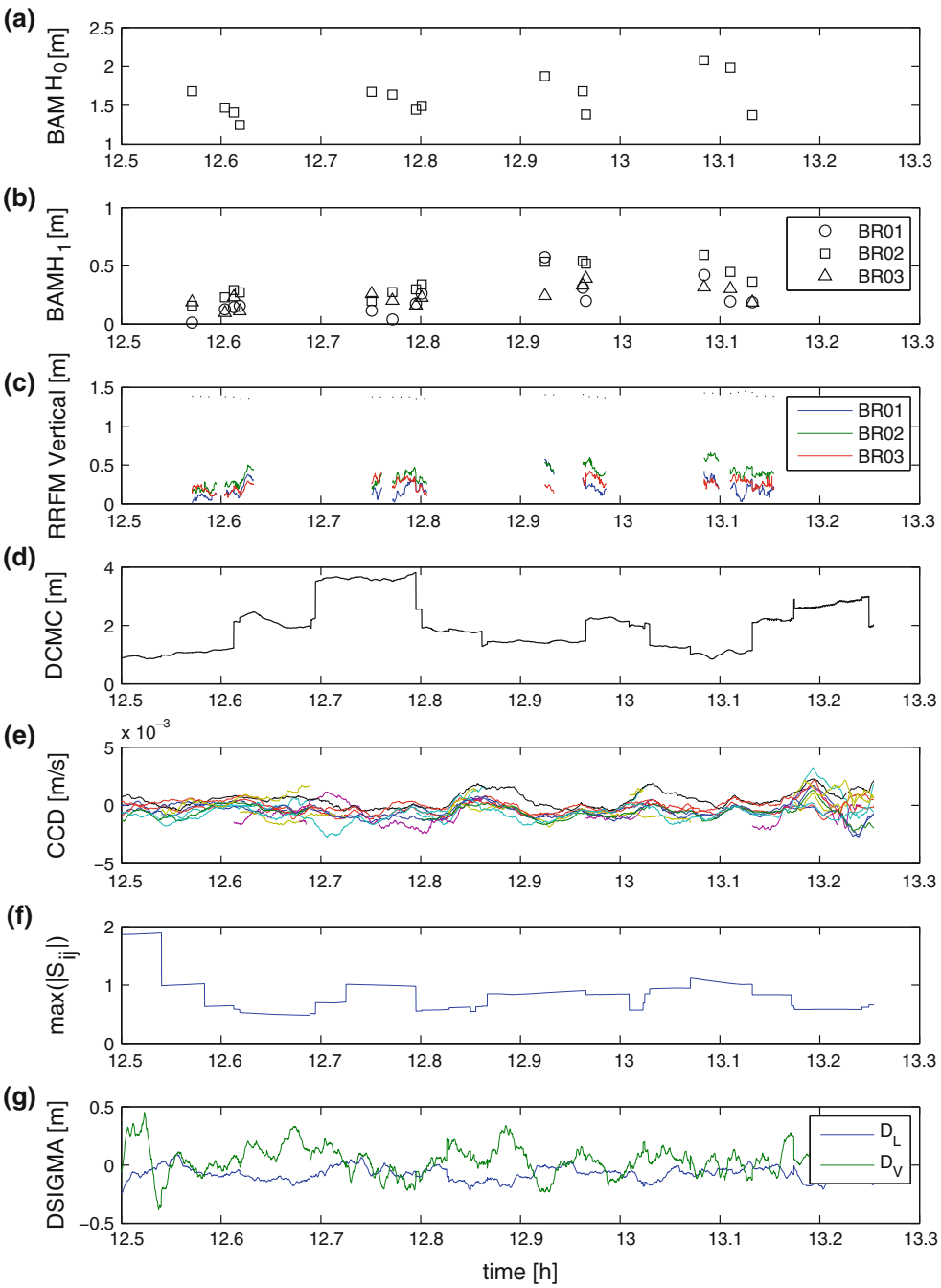

Fig. 8 Monitor output during the flight experiment of November 27, 2009: **a** H_0 component of the BAM, Eq. (29). **b** H_1 component of the BAM, Eq. (30). **c** Vertical component of the RRFM and the associated threshold (*dotted line*). **d** DCMC without the satellite clock corrections. **e** CCD for all satellites that were used in the position computation. **f** Maximum element of the GAST-D pseudoinverse S. **g** DSIGMA vertical and lateral position differences D_L and D_V before taking the absolute value

vertical biases. The first evaluation determines whether the 66% nominal error bound is smaller than FASVAL

$$2\sqrt{\sum_{i=1}^{N} S_{\mathrm{Apr,vert},i}^2 \sigma_i^2} + D_V < \mathrm{FASVAL} \tag{29}$$

Secondly, each ground station receiver is checked for biases using

$$\left|\sum_{i=1}^{N} S_{\mathrm{Apr,vert},i} B(i,j)\right| + D_V < \mathrm{FASVAL}. \tag{30}$$

Reference receiver fault monitor (RRFM)

In addition to the ground station, the GAST-D airborne subsystem, while inside the precision approach region, also performs a continuous monitoring of the ground station reference receivers by means of the received B-values. Similar to the bias approach monitor, the RRFM uses

$$\left|\sum_{i=1}^{N} S_{\mathrm{Apr,vert},i} B(i,j)\right| + D_V < T_{\mathrm{B,air,vert}} \tag{31}$$

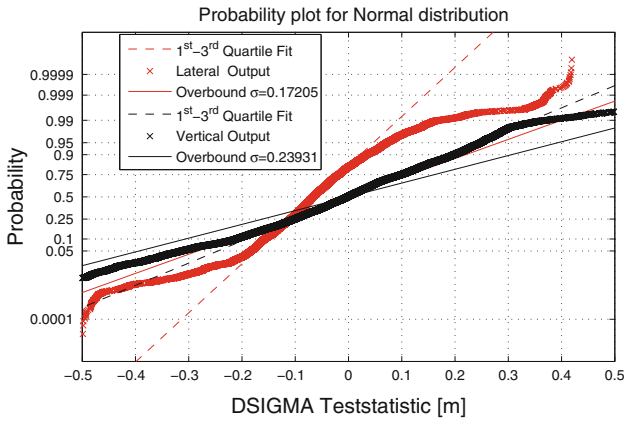

Fig. 9 Overbound of the DSIGMA data collected during the flight trials. The vertical data are shown in *black*, the lateral in *red*

$$\left|\sum_{i=1}^{N} S_{\mathrm{Apr,lat},i} B(i,j)\right| + D_{\mathrm{L}} < T_{B,\mathrm{air,lat}} \tag{32}$$

with two computed thresholds

$$T_{B,\mathrm{air,vert}} = K_{\mathrm{ffd},B}\sqrt{\sigma^2_{B_{\mathrm{vert}}} + \sigma^2_{D_{\mathrm{V}}}} \tag{33}$$

$$T_{B,air,lat} = K_{ffd,B}\sqrt{\sigma^2_{B_{lat}} + \sigma^2_{D_L}} \tag{34}$$

The standard deviations for D_{L} and D_{V} are precalibrated by the air subsystem manufacturer. The σ_{B_lat} and σ_{B_vert} are given by

$$\sigma^2_{B_{\mathrm{vert}}} = \sum_{i=1}^{N} \frac{S^2_{\mathrm{Apr,vert},i}\sigma^2_{\mathrm{pr,gnd},i;100}}{U(i)} \tag{35}$$

$$\sigma^2_{B_{\mathrm{lat}}} = \sum_{i=1}^{N} \frac{S^2_{\mathrm{Apr,lat},i}\sigma^2_{\mathrm{pr,gnd},i;100}}{U(i)} \tag{36}$$

where $U(i)$ is the number of reference receivers used to compute the B-values and usually equal to $M-1$. The first test is essentially the same as the one performed for the bias approach monitor, only the threshold is slightly different.

Measurement quality monitor

The required measurement quality monitor is a cycle slip detector based on the 30 s smoothed pseudoranges. The magnitude of the difference of projected pseudorange

$$\hat{\rho}_{\mathrm{projected}} = \hat{\rho}_{n-1} + \frac{\lambda}{2\pi}(\phi_n - \phi_{n-1}) \tag{37}$$

and raw pseudorange ρ_n is compared to a 10 m threshold,

$$|\rho_n - \hat{\rho}_{\mathrm{projected}}| < 10 \tag{38}$$

If the threshold is exceeded, the smoothing filter is reinitialized.

Reference trajectory

As a reference for the position output, we post-processed dual frequency L1 and L2 carrier phase data using GrafNav 7.8 from Novatel (http://www.novatel.com) in a combined forward and reverse solution. The ambiguity resolution was initialized by a one-minute static segment before each flight. As reference stations, we chose the three GBAS ground sites (Table 1) that also recorded code and carrier phase on L1 and L2.

Results

Figure 5 shows the temporal evolution of the vertical integrity data during the flight trial on 11-27-2009. In general, both GAST-C and GAST-D protection levels follow the same pattern—albeit the GAST-D VPL is noisier due to the addition of D_{V}. Due to the behavior of the σ_i as mentioned in Sect. 3, the $\mathrm{VPL}_{\mathrm{GAST}-D}$ is not always larger than the $\mathrm{VPL}_{\mathrm{GAST}-C}$ despite the addition of D_{V}. However, the structure of Eqs. 21 and 25 is chosen such that at the final approach segment, $\mathrm{VPL}_{\mathrm{GAST}-D}$ always becomes larger than $\mathrm{VPL}_{\mathrm{GAST}-C}$. This is visible in Fig. 5 and is marked with black circles. For this flight experiment, the position error of the airborne subsystem does not exceed 1.85 m.

Figure 6 top and bottom are vertical and lateral integrity plots for the GAST-D service based on the data of all flight experiments, while the aircraft was inside the precision approach region. The integrity plot can be divided into four areas: For normal operations, the position error is smaller than the protection level, which is in turn smaller than the alert limit (white area). The system is available and overbounding the actual position error correctly. If the protection level is larger than the alert limit, the system is unavailable for use (yellow area). Should the position error exceed the protection level, misleading information is given by the system (red/pink area). In case the navigation system error is larger than the alert limit, this misleading information becomes hazardous to the aircraft (red area) since no guarantee for it to be within the protected area can be given. For the evaluation of the flight trial data, we normalized both axes using the alert limit at a given time, since the alert limits vary with distance. During the 30 approaches, we collected 31,424 data samples at 2Hz inside the approach area and 16,012 data samples inside the precision approach region. In order to assess integrity for all flight trials, data were used only when the aircraft was in the precision approach area for runway 26 as depicted in Fig. 7. We used the minimum GBAS approach service volume as given in RTCA DO245A, which extends at an angle of 7° up to 10,000 ft above ground level to a distance of 20 nm within

35° of the runway centerline and the precision approach region that extends within ±5° up to five miles from the landing threshold point (LTP). At no time, misleading information or hazardously misleading information occurred and the system was available all the time during all approaches. As expected, both navigation system error and protection level for the vertical component are larger and have a wider distribution than the lateral component.

During all flight trials, no alarm was triggered by any of the monitors. As an example of the monitor performance, we show the output of all GAST-D airborne monitors during the flight experiment of November 27, 2009 in Fig. 8.

Figure 8a, b shows the results for the bias approach monitor for the H_0 hypothesis as described by (29) and the H_1 hypothesis as described by (30), respectively. Figure 8c shows the test statistic of the vertical component of the reference receiver fault monitor (31) and the associated threshold (33). Since four approaches were conducted that day, the BAM and RRFM were activated four times—when the aircraft was inside the precision approach region. Figure 8d displays the magnitude of the horizontal projection of the differential corrections without the satellite clock corrections. Figure 8e contains the test quantity of the code-carrier divergence monitor as described by (7) for all satellites that were used in the position computation. The maximum element of the GAST-D pseudoinverse S is given in Fig. 8f with a maximum value of 1.89. Figure 8g shows the DSIGMA vertical and lateral position differences D_L and D_V before taking the absolute value. The absolute maxima and minima are 0.24 m laterally and 0.45 m vertically. The empirical distribution of the collective output of the DSIGMA monitor while the aircraft was within the service area is shown in Fig. 9. An overbound of the two empirical distributions in the quantile domain (Dautermann et al. 2012) yields standard deviations of $\sigma_L = 0.17205\text{m}$ and $\sigma_V = 0.23931\text{m}$. These are about the same as the ones found by Murphy and Harris (2006) through first-third quartile fits.

Conclusions

Here, we have shown an evaluation of GPS data recorded during flight trials in 2009. Since we only evaluated flight trial data during nominal conditions, no failure modes or specific threats to the GAST-D GBAS system were addressed or observed. The DLR GBAS testbed is currently being upgraded to support the GAST-D standards set forth in the ICAO GAST-D SARPs and RTCA DO253C in real time. As opposed to post-processing, additional effort must be put into data transport and the timely processing of corrections. We have demonstrated that GAST-D performance is possible with the existing infrastructure. Had a GAST-D real-time architecture been operational during the 2009 flight trials, all approaches could have successfully been completed in accordance with the standards valid at the time this analysis was performed. Several issues still remain before a fully certified GAST-D system will be available for commercial use. The SARPs require an absolute ionospheric gradient monitor to protect the aircraft from range biases of up to 1.5 m at the threshold. A $\sigma_{\text{vert\_iono\_gradient},D}$ will need to be determined using data for the area for which certification is sought. Lastly and most importantly, inconsistencies within the standards need to be clarified and eliminated.

The DLR GBAS testbed with its completely modifiable architecture permits research and demonstration of new algorithms. Other DLR facilities such as the Multi-output Advanced Signal Test Environment for Receivers (Dautermann et al. 2010) can be used in conjunction with the GBAS testbed to simulate threats and worst-case situations in support for standardization and certification.

Acknowledgments We would like to thank the DLR Aviation Directorate for funding the TOPGAL project. We thank Boubeker Belabbas for managing the project across the different DLR Institutes.

References

Burns J, Clark B et al. (2009) Conceptual framework for the proposal for GBAS to support CAT-III operations, ICAO Navigation Systems Panel

Cohen CE, Cobb HS, Lawrenc DG, Pervan BS, Powell JD, Parkinson BW, Aubrey GJ, Loewe W, Ormiston D., McNally BD, Kaufmann DN, Wullschleger V, Swider R (1995) Autolanding a 737 using GPS and integrity beacons. In: Proceedings of digital avionics systems conference, 1995, 14th DASC, pp 475–482, doi: 10.1109/DASC.1995.482940

Datta-Barua S, Walter T, Pullen S, Luo M, Blanch J, Enge P (2002) Using WAAS ionospheric data to estimate LAAS short baseline gradients. In: Proceedings of ION 2002 national technical meeting

Dautermann T, Mayer C (2010) Equatorial plasma depletions observed over Brazil—impact on safety critical GNSS navigation. In: Proceedings of the 23rd international technical meeting of the satellite division of the institute of navigation (ION GNSS 2010), Portland, OR

Dautermann T, Remi P, Belabbas B, Pullen S. (2010) GBAS ionospheric threat analysis using DLRs hardware signal simulator. In: Proceedings of the ESA Navitec 2010, Nordwijk, Netherlands

Dautermann T, Mayer C, Belabbas B, Antreich F, Konovaltsev A, Kaelberer U (2012) Non-Gaussian error modeling for GBAS integrity assessment. In: IEEE transactions on aerospace and electronic systems (in press)

Enge P (1999) Local area augmentation of GPS for the precision approach of aircraft. Proc IEEE 87(1):111–132. doi:10.1109/5.736345

EUROCAE ED114 (2003), Minimum operational performance specification for global navigation satellite ground based augmentation system ground equipment towards support category I operations. Tech. Rep. ED-114, EUROCAE

FAA (2003), Airworthiness approval of global navigation satellite system (GNSS) equipment, advisory circular information AC20-138A

FAA (2005), Category I local area augmentation system ground facility—NON-FED specification, NON-FED Specification FAA-E-AJW44-2937A, Federal Aviation Administration

Gratton L, Pervan B, Pullen S (2004) Orbit ephemeris monitors for category 1 LAAS. IEEE, pp 429–438

Honeywell (2009) Honeywell Smartpath precision landing system first to receive FAA system design approval

ICAO NSP (2010), GBAS CAT II/III development baseline SARPs, International Civil Aviation Organization

IS-GPS-200D (2004), Navstar GPS Joint Program Office (SMC/GP) Navstar GPS space segment/navigation user interfaces

Khanafseh S, Yang F, Pervan B, Pullen S, Warburton J (2010) Carrier phase ionospheric gradient ground monitor for GBAS with experimental validation. In: Proceedings of the 23rd international technical meeting of the satellite division of the institute of navigation (ION GNSS 2010), Portland, OR, pp 2603–2610

Lee J, Pullen S, Xie G, Enge P (2001) LAAS sigma-mean monitor analysis and failure-test verification. In: Proceedings of the 57th annual meeting of the institute of navigation, pp 694–704

Lee J, Pullen S, Datta-Barua S, Enge P (2007) Assessment of ionosphere spatial decorrelation for global positioning system-based aircraft landing systems. J Aircraft 44(5):1662–1669. doi: 10.2514/1.28199

Luo M, Pullen S, Akos D, Xie G, Datta-Barua S, Walter T, Enge P (2002) Assessment of ionospheric impact on LAAS using WAAS supertruth data. In: Proceedings of the 58th annual meeting of the institute of navigation and cigtf 21st guidance test symposium, pp 175–186

Luo M, Pullen S, Walter T, Enge P (2004), Ionosphere spatial gradient threat for LAAS: mitigation and tolerable threat space. In Proceedings of the 2004 national technical meeting of the institute of navigation, pp 490–501

McGraw GA, Murphy T, Brenner M, Pullen S, Van Dierendonck AJ (2000) Development of the LAAS accuracy models. In Proceedings of the 13th international technical meeting of the satellite division of the institute of navigation, pp 1212–1223

Mitelman A, Jung J, Enge P (1999) LAAS monitoring for a most evil satellite failure. In: Proceedings of the 1999 national technical meeting of the institute of navigation. San Diego, CA, pp 129–134

Murphy T, Harris M (2006) Mitigation of ionospheric gradient threats for GBAS to support CAT II/III. In: Proceedings of the 19th international technical meeting of the satellite division of the institute of navigation (ION GNSS 2006), Fort Worth, TX, pp 449–461

Murphy T, Ackland J, Imrich T, Lapp T, Friedman R (2006) Early operational experience with new capabilities enabled by GBAS landing systems (GLS). In: Proceedings of the 2006 national technical meeting of the institute of navigation. Monterey, CA, pp 468–478

Murphy T, Harris M, Beauchamp S (2010) Implications of 30-second smoothing for GBAS approach service type D. In Proceedings of the 2010 international technical meeting of the institute of navigation. San Diego, CA, pp 376–385

Ndili A (1994) GPS pseudolite signal design. In: Proceedings of the 7th international technical meeting of the satellite division of the institute of navigation (ION GPS 1994), Salt Lake City, UT, pp 1375–1382

Normark PL, Akos D, Xie G, Pullen S, Luo M, Enge P (2002) The integrity monitor testbed and multipath limiting antenna test results. In: Proceedings of the 15th international technical meeting of the satellite division of the institute of navigation. Portland, OR, pp 2596–2601

Pervan B, Chan FC (2003) Detecting global positioning satellite orbit errors using short-baseline carrier-phase measurements. J Guid Control Dyn 26(1):122–131

Pullen S (2000) Summary of ionosphere impact on PT 1 LAAS: performance and mitigation options. Stanford University, Dept. of Aeronautics and Astronautics, Stanford

Pullen S, Luo M, Xie G, Lee J, Phelts RE, Akos D, Enge P (2002) LAAS ground facility design improvements to meet proposed requirements for category II/III operations. In: ION GNSS

RTCA DO245A (2004) Minimum aviation system performance standards for the local area augmentation system (LAAS), Tech. rep., DO245A, RTCA

RTCA DO253C (2008) Minimum operational performance standards for GPS local area augmentation system airborne equipment, Tech. Rep. DO253C, RTCA

RTCA DO246D (2009) GNSS based precision approach local area augmentation system (LAAS) signal-in-space interface control document (ICD), Tech. rep. DO246D, RTCA

Satkunanathan L, Murphy T (1998) Satellite-based guidance for precision approach and landing of commercial airplanes. GPS Solut 2:21–26

Shively CA, Hsiao TT (2010), Availability of GAST D GBAS considering continuity of airborne monitors. In: Proceedings of the 2010 international technical meeting of the institute of navigation. San Diego, CA, pp 365–375

Simili DV, Pervan B (2006) Code-carrier divergence monitoring for the GPS local area augmentation system. In: Proceedings of the position, location, and navigation symposium, pp 483–493